European Wind Energy Conference & Exhibition 2009
Parc Chanot, Marseille, France 16-19 March 2009

ACTIVE AERODYNAMIC BLADE CONTROL DESIGN FOR LOAD REDUCTION ON LARGE WIND TURBINES

David G. Wilson*, Dale E. Berg, Mathew F. Barone, Jonathan C. Berg, Brian R. Resor and Don W. Lobitz
Energy Systems Analysis*/ Wind Energy Technology
Sandia National Laboratories, P.O. Box 5800
Albuquerque, New Mexico 87185–1108
Email: {dwilso,deberg,mbarone,jcberg,brresor,dwlobit}@sandia.gov

ABSTRACT

Through numerical simulations that use trailing edge flaps as active aerodynamic load control devices on wind turbines that range from 0.6MW-5MW rated power, a 20-32% reduction in blade root flap bending moments was achieved. This allows the turbine blade lengths to be increased, without exceeding original fatigue damage on the system, resulting in larger swept rotor area. This study developed and simulated several independent flap control designs (including tip deflection and tip rate deflection feedback) that seamlessly integrated with existing pitch control strategies to reduce loads sufficiently to allow 10% rotor extension and increased energy capture (see reference [1] for methodology).

1 Introduction

Wind turbines are large, complex, dynamically flexible structures that must operate under very turbulent and unpredictable environmental conditions where efficiency and reliability are highly dependent upon a well-designed control strategy. The possibility to quickly influence aerodynamic loads acting on the individual blades allows for a hybrid pitch control objective that includes a high frequency dynamic attenuation component with respect to fatigue load reduction. Active aerodynamic devices are potential candidates for this component.

With wind turbine blades getting larger and heavier, can the rotor weight be reduced by adding active devices? Can active control be used to reduce fatigue loads? Can energy capture in low wind conditions be improved? These are some of the questions that are being addressed in our research program. Specifically, our research goal is to understand the implications and benefits of active blade control in Region III, defined as windspeeds between V_{rated} to $V_{cut-out}$ and Region II, defined as windspeeds between V_{cut-in} to V_{rated} (as shown in Fig. 1), respectively. In this study Region III is the region of interest.

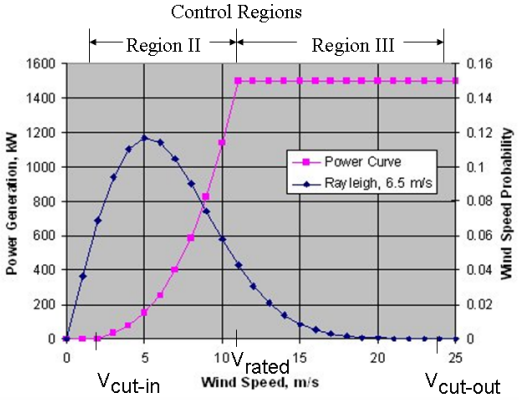

Figure 1. Control Regions for a typical Wind Turbine

To modify the blade/turbine active load control one can change blade aerodynamic characteristics through: i) surface blowing/suction, ii) VG's, surface heating, plasma, etc., or iii) changes in section shape (aileron, smart materials, microtabs). In this work the last approach is taken.

In practical applications the reduction of structural fatigue loads is important for the continued operation of wind turbines over a lifetime. One example of these types of loads is reported by Kelley, et.al. [2], where the impact of coherent inflow turbulence on the wind turbine dynamic response is identified.

*Address all correspondence to this author.

Previous field experimentation showed greatest structural fatigue damage tends to occur during nighttime hours from coherent turbulence that develops in the stable, nocturnal atmospheric boundary layer. Under such conditions, intense vertical wind shear and temperature gradients create resonant flow fields capable of imparting short-period loading and vibrational energy as wind turbine rotor blades pass through regions of organized or coherent turbulence. This energy is subsequently propagated throughout the remainder of the structure, where it is often locally dissipated [2].

In this particular case, a time-frequency spectral decomposition of the blade root flapwise load resulting from encountering coherent turbulent structure indicated that the highest level of dynamic stress energy occurred in the frequency range consisting of the first and second flap bending modes [2, 3]. It was determined that the number of stress reversals increase as the rotor passes through coherent turbulent structures [2]. Due to the nature of the load application and the existence of small values of structural damping, a potentially significant transient storage of vibrational energy must be dissipated. Potentially, a modal dynamic amplification could contribute to a lower than designed component service lifetime [2]. Active aerodynamic devices are a good candidate to help reduce these detrimental effects of high frequency dynamics and fatigue loads on wind turbines.

For wind turbines to continue a reduction in cost of energy, technical advances from several areas will be required. In the area of aerodynamics, controls, and sensors, several researchers have started to investigate the benefits of using advanced control for wind turbine rotor aerodynamics and geometry. In McCoy and Griffin [4], two major categories of rotor aerodynamic modifications were investigated; active aerodynamic devices and actively controlled retractable blade rotors. Both studies showed indications of cost savings through reduced system loads and increased energy capture. Van Dam et. al. [5–7], have investigated, both computationally with CFD investigations and through experimental wind tunnel testing, the feasibility of using microtabs for active load control. Andersen, et.al. [8] have developed deformable trailing edge geometry and control algorithms which also showed fatigue load reduction for both the flapwise blade root moments and the tower root moments. By enabling the trailing edge at the outboard portion of the blade to move quickly and independently, local fluctuations in the aerodynamic forces can be compensated. Additionally, Barlas and van Kuik [9] give an overview of smart rotor control technology for wind turbines.

In this study the authors investigate the combined control performance of several types of trailing-edge devices that include micro-tabs, morphing trailing edges (5%, 10%, 20% of blade chord), and conventional trailing edge flaps in conjunction with collective pitch control to provide effective load alleviation for a range of variable-speed, variable-pitch wind turbines (600 kW NREL CART [10], 1.5MW WindPACT [11], and 5.0 MW NREL Offshore [12]). This study demonstrates that advanced independent flap control based on either tip deflection or tip deflection rate measurements, combined with existing blade pitch control strategies, is advantageous for loads reduction. In addition, the control designer must be aware of and keep to a minimum the flap bending and torsion coupling which may become more apparent as the turbines increase in rotor diameter.

This paper is divided into six sections. Section 2 provides an overview of the active aerodynamic devices and performance employed on the wind turbines. Section 3 defines the three wind turbine models. Section 4 develops the hybrid control system for both the pitch and active aerodynamic controllers. Section 5 presents the numerical simulation results for the three wind turbines studied and Section 6 summarizes the results with concluding remarks.

2 Active Aerodynamic Devices and Performance

2.1 Characteristics

The aerodynamic properties of blade sections with active aerodynamic devices required by the FAST code were obtained using the ARC2D code [13] Computational Fluid Dynamics (CFD) code. The ARC2D code, a two-dimensional Navier-Stokes solver, was used to generate aerodynamic lookup tables for lift coefficient, drag coefficient, and pitching moment coefficient for each airfoil geometry of interest, including configurations where the microtab or morphed shape was activated. The CFD results were obtained using the Spalart-Allmaras turbulence model, with specified upper and lower surface boundary layer transition locations. The transition locations were estimated using the XFOIL viscous panel code [14]. The use of CFD allowed for a consistent method for determining changes in airfoil performance with the non-trivial shape changes associated with the active aerodynamic devices. The time required to generate meshes for the CFD calculations of many different shapes was greatly reduced by the use of an automated mesh-generation tool [15]. CFD solutions were obtained over an angle of attack range of -14 degrees to +20 degrees; the airfoil tables were then pre-processed using the AirfoilPrep spreadsheet [16], which applies the Viterna method to expand the performance tables to the full 360 degree range of angles of attack required by the FAST/Aerodyn codes. The next subsections discuss the unique features of each active aerodynamic device.

2.2 Microtab concepts and background

The microtab concept comes from an evolutionary development of the Gurney flap (see Liebeck [17]). The tab is deployed near the trailing edge of the airfoil to a height on the order of the boundary layer thickness (approximately 1% of chord), as shown in Fig. 2. Some of the desirable features include: i) significant

increases in C_L, ii) relatively small increase in C_D, and iii) proper sizing can increase L/D. Further details of the microtab concept can be found in reference [18].

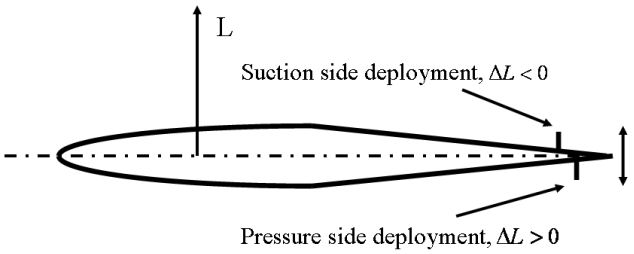

Figure 2. Microtab concept based on Kutta Condition (van Dam [18])

The specific microtab characteristics, based on experimental results, are given in Fig. 3 for both the lift and drag profiles, respectively. These profiles are typical of those used as AeroDyn [19] inputs to the FAST/Simulink [20] dynamics and controls simulator.

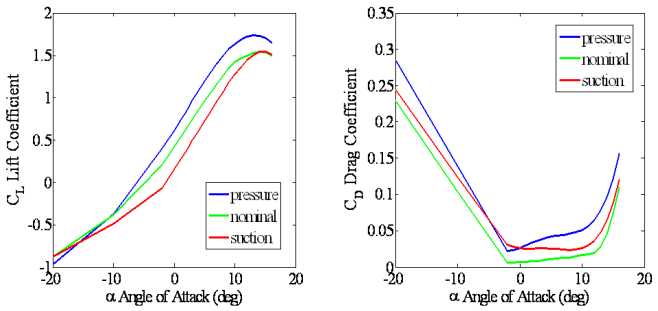

Figure 3. Microtab C_L and C_D Profiles used as input to AeroDyn software

2.3 Morphing wing concept

FlexSys Inc., of Ann Arbor, Michigan has developed and flight tested a technology that enables them to morph a wing trailing edge [21, 22]. That is, they can smoothly and quickly distort the trailing edge of a wing to form an effective flap, while avoiding the discontinuities in the upper and lower wing surfaces, the hinge line and the attendant air gap that are associated with traditional flaps. The morphed flap has a lift characteristic comparable to that of a conventional flap, but with a much reduced drag increment due to flap deflection. Morphing wing cross-section profiles for a 10% chord flap are shown in Fig. 4.

2.4 Conventional trailing edge flaps

An airfoil with a conventional flap consists of two distinct sections - the fixed leading edge section of the airfoil and a rigid

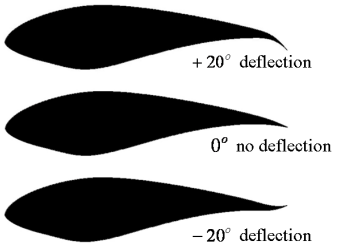

Figure 4. Morphing wing trailing edge concept ([21])

trailing edge section that rotates about the spanwise hinge attached to the leading edge section (see Fig. 5). This type of flap has a distinct hinge line, an associated clearance gap (through which air can leak, causing loss of lift and generating noise) and sharp changes or discontinuities in both the upper and lower surfaces of the airfoil. As a result of these characteristics, the airflow over the airfoil with a deflected flap tends to separate at low angles of attack and create more drag than a morphing trailing edge.

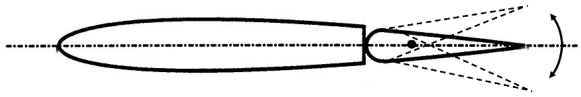

Figure 5. Conventional trailing edge airfoil

3 Wind Turbine Models

The wind turbine structural models utilized in this work are in the public domain and include the NREL 600 kW 2-bladed Controls Advanced Research Turbine (CART) [10], the 1.5 MW WindPACT turbine [11], and the NREL/UpWind 5 MW Offshore wind turbine [12] (see Table 1). All turbines are upwind, with variable rotational speed, and collective pitch control. The NREL FAST/AeroDyn/Simulink [20] wind turbine dynamics/controls simulation code is employed for all control system numerical simulation studies.

In general terms, the FAST aero-elastic nonlinear dynamics model can be represented as a nonlinear first-order input-ouput system

$$\begin{aligned} \dot{\mathbf{x}} &= \mathbf{f}(\mathbf{x}, \mathbf{u}, \mathbf{u_d}) \\ \mathbf{y} &= \mathbf{g}(\mathbf{x}, \mathbf{u}, \mathbf{u_d}) \end{aligned} \tag{1}$$

where $\mathbf{u}$ is the vector of control inputs, $\mathbf{u_d}$ is the vector of disturbance inputs (wind), $\mathbf{x}$ is the state vector, and $\mathbf{y}$ is the measurement vector. The maximum number of variables for the FAST simulator is extensive and the interested reader is referred to the FAST software and documentation [20], for complete details. In this development only the specific variables of interest will be discussed.

In Region II (from V_{cut-in} to V_{rated}), the wind turbines operate at variable rotation speeds [23]. A popular industrial standard control law (also implemented in the baseline FAST models), commands the generator torque as

$$\mathbf{u} = u_{gt} = k\Omega^2 \tag{2}$$

where $k = 1/2\rho AR^3 C_{P_{max}}/\lambda_*^3$. The symbols are defined as: Ω the generator rotational speed, ρ the air density, A the rotor swept area, R the rotor radius, $C_{P_{max}}$, the maximum aerodynamic power coefficient, corresponding to λ_* the optimal tip speed ratio, for a particular blade pitch angle. The controller gain k is often determined from wind turbine aerodynamic performance analysis. The standard baseline values were used for each respective turbine in this study.

As discussed by Wright [10], the goal of Region III is to regulate rotor speed to a certain set point by using blade pitch to control rotor speed while maintaining constant generator torque. Typically, a simple linear model is used for the control design as is given by [10]

$$\Delta\dot{\Omega} = A\Delta\Omega + B\Delta\Theta + B_d\Delta w \tag{3}$$

where A, B, and B_d are functions of the total rotational inertia due to the rotor, gearbox, shafts, generator, etc. and the sensitivity of the rotor aerodynamic torque with respect to Ω, Θ, and w, respectively. Note that Ω has been previously defined, Θ is the blade pitch angle, and w is the hub-height uniform wind speed disturbance across the rotor disk. The baseline Proportional-Integral-Derivative (PID) rotor collective pitch control expression to regulate turbine speed is given by [10]

$$u_i = \Delta\Theta_i(t) = k_{P_i}\Delta\Omega_i(t) + k_{I_i}\int_0^t \Delta\Omega_i(t)dt + k_{D_i}\Delta\dot{\Omega}_i(t) \tag{4}$$

for $i = 1$ to n_{blades}. The PID control gains, k_P, k_I, and k_D have been determined approporiately to maintain a stable, closed-loop system with a critically damped reponse. For each of the wind turbine models, the baseline pitch control systems, existing in the FAST models, have been used for all these numerical simulations. The transition from Region II to Region III is typically called Region II 1/2. The baseline FAST Region II 1/2 control is automatically used for each wind turbine in this study.

Each wind turbine has been modified to include an Active Aerodynamic Load Control (AALC) system to work with the existing collective pitch control system (see Table 1). The next section will discuss the hybrid pitch/AALC system in more detail.

Table 1. Wind turbine model characteristics

Turbine	CART [10]	WindPACT [11]	Offshore [12]
Rating	600kW	1.5 MW	5.0MW
Rotor size	42.7m	65.9m	126m
Blade len.	20.0m	31.3m	61.5m
V_{rated}	13 mps	12.5 mps	11.4 mps
$V_{cut-out}$	20 mps	22.5 mps	25 mps
n_{blades}	2	3	3
AALC	microtabs	morphing wing	conventional flaps
β_{limit}	$\pm$1(max)	$\pm 10^\circ$	$\pm 10^\circ$
$\dot{\beta}_{limit}$	—-	75 °/sec	75 °/sec

4 Hybrid Pitch/Active Aero Control System Design

In Region III, most wind turbines have a collective pitch control scheme to keep the turbine operating at peak output power while at higher wind speed conditions. One of the initial goals of the current project was to minimize the redesign of the control system, yet understand the benefits of introducing active aerodynamic devices on the blades. Therefore, a hybrid controller that combines a traditional pitch control system with the microtab, morphing wing, or conventional flap control system was developed. The collective pitch control system consists of an existing PID feedback design [10, 24] as shown in Eq. (4) as part of all the wind turbines that were investigated. The active aerodynamic devices all use the same control system structure, consisting of a Proportional-Derivative (PD) feedback design, similar to the one discussed in [25]. The PD controller uses tip deflection as the feedback signal or

$$\mathbf{y} = [y_{tip_1} \quad y_{tip_2} \quad y_{tip_3}]^T, \tag{5}$$

in addition to what is normally feedback in the baseline FAST simulator for collective pitch control, etc. (For the CART 2-bladed model, there are only two tip deflection signals). This measurement vector assumes both availability and ideal sensor feedback from the FAST output with no time delay. In addition, a nominal operating point, $y_{tip_{nom}}$, is included as a reference input signal. The reference input signal is determined by finding the mean value of the tip deflection for the basline run without AALC. In the future, this signal will be generated based on a running real-time average formulation. Next, an error signal is formulated as $e = (y_{tip} - y_{tip_{nom}})$ for which the control law be-

comes

$$u_{i+n_{blades}} = \beta_{actuator_i} = -K_{P_i} e_i - K_D \dot{e}_i \tag{6}$$

for $i = 1$ to n_{blades}. Here $\beta_{actuator}$ is either the deployment signal (microtabs) or the rotational deployment of the morphing wing or the conventional flap deflection angle, K_P is the proportional gain, and K_D is the derivative gain. For this work, the active aerodynamic devices are considered fast-acting and capable of responding to high frequency disturbances. Therefore, the augmentation with the existing low frequency blade collective pitch control has been seamless, as though decoupled from each other (i.e., partitioned high-frequency/low-frequency control).

In the AALC controller design, the controller gains were selected to optimize maximum power ouput while minimizing blade root flap bending moment oscillations about a mean during turbulent wind conditions. This performance criteria was subject to the requirements to minimize actuator saturation, $|\beta_{actuator}| \leq \beta_{actuator_{MAX}}$, and remain within actuator maximum rate specifications, $\left|\dot{\beta}_{actuator}\right| \leq \dot{\beta}_{actuator_{MAX}}$, (see Table 1 for limits).

The actual AALC signal sent to FAST is implemented through the C_D and C_L aerodynamic load profiles (for example, see Fig. 3). The aerodynamic loads are applied through the Blade Element Momentum nodes for each blade. In each of the wind turbine cases, the outer 25% of the blade is considered to have AALC capability. Three sets of profiles (pressure-side maximum deployed, neutral, suction-side maximum deployed) are then implemented for this 25% portion of the wind turbine blade. For a calculated controller output value that is between the limits, interpolation is performed within the aerodynamic profiles to determine the corresponding aerodynamic loads to be applied at that instant in time. This interpolation feature is an internal capability within the Aerodyn/FAST interface software. This is considered as a first-order effect implementation. The integration of these AALC devices within the structure and their local deformation responses have not been considered.

Rate feedback controller: The implementation of rate feedback control assumes that the tip deflection rate measurement signal is available or easily reconstructed from either a tip accelerometer or a tip deflection sensor or

$$\mathbf{y} = [\dot{y}_{tip_1} \quad \dot{y}_{tip_2} \quad \dot{y}_{tip_3}]^T, \tag{7}$$

in addition to what is normally feedback in the baseline FAST simulator for collective pitch control, etc. (For the CART 2-bladed model, there would only be two tip deflection rate signals). In this case, the control law is defined as

$$u_{i+n_{blades}} = \beta_{actuator_i} = -K_{V_i}\, \dot{y}_{tip_i} \tag{8}$$

for $i = 1$ to n_{blades} and K_V is the rate feedback control gain. This second control law was also separately tested on the 1.5MW WindPACT machine and it acts as a regulator with respect to tip deflection rate. In other words, the ideal or nominal tip deflection rate value would be zero (no motion). Each control law with either tip (deflection or rate) feedback was shown to be effective in alleviating loads.

5 Numerical Simulation Results

The FAST/Simulink modeling environment [20] was used to evaluate the hybrid control system performance at 18 mps wind condition in Region III (see Fig. 6 for actual rotor centerline IEC turbulent wind conditions used in these simulations). Several 10 min turbulent wind conditions were investigated. For these discussions a time splice of 100 seconds is displayed in all the time domain responses shown in the Appendix.

The baseline CART FAST model was modified to incorporate the microtab control system as shown in Fig. 7. The block in green is the CART plant, while all the control system feedback loops are implemented in the Simulink block diagram (see Fig. 7). The same process was used for the 1.5MW WindPACT wind turbine utilizing the morphing wing trailing edge devices with 20% blade chord modifications. For the 5MW offshore wind turbine, conventional flaps were employed.

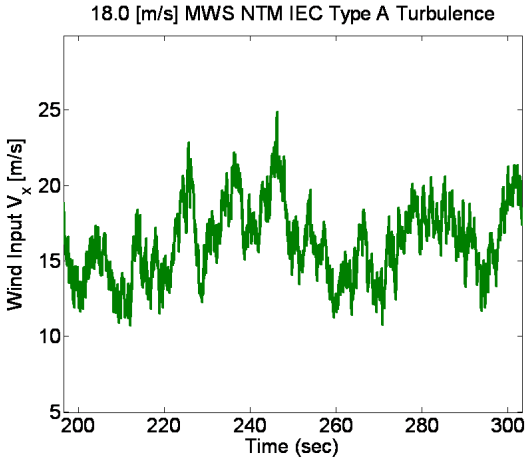

Figure 6. Wind input file used for all WT discussions and applied at turbine hub.

5.1 600kW CART machine [10]

The numerical simulation results from the FAST runs are reported for both *MicroTabs* (shown in blue) and *No MicroTabs* (shown in red) cases. Figure 10 (in Appendix) shows the blade 1 root flap moment response (first row -left) and the blade tip deflection response (first row - right). For the root flap moment a

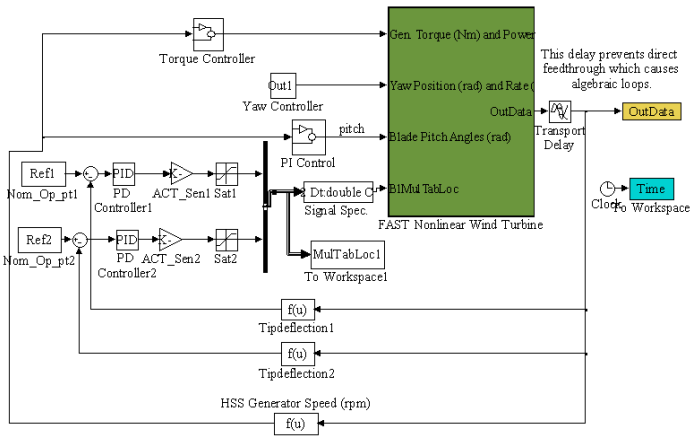

Figure 7. Dynamic simulation environment: FAST with augmented pitch and microtab control systems for the CART machine

reduction of the peak moments of 21%, along with a reduction in overall tip deflection can be observed (see Table 2).

Figure 10 (in Appendix) also shows the blade 1 pitch angle responses (second row - left) along with the microtab sequencing output (second row - right). Figure 10 (in Appendix) shows the generator power response (third row - left) and the rotor speed response (third row - right); both power and speed are maintained while using microtabs.

Since the combined control systems can potentially couple other degrees-of-freedom associated with the overall system, the tower modes were also checked. Figure 10 (in Appendix) shows the tower base side-to-side moment response (fourth row - left) and the tower base fore-aft moment response (fourth row - right). The presence of microtabs has no effect. In addition, the LSS torque (see Fig. 10 last row - left, in Appendix) and tower top/yaw bearing yaw moment (last row - right) responses demonstrate that these loads remain level while activating the AALC devices.

5.2 1.5MW WindPACT wind turbine [11]

Tip deflection feedback: The numerical simulation results from the FAST runs are reported for both morphing wing with 20% blade chord *Flaps 20% C* (shown in blue) and no morphing *No Flaps* (shown in red) cases. Figure 11 (in Appendix) shows the blade 1 root flap moment response (first row - left) and the blade tip deflection response (first row - right). For the root flap moment a reduction of the peak moments of 32%, along with a reduction in overall tip deflection, can be observed (see Table 2). Figure 11 (in Appendix) shows the blade 1 pitch angle responses (second row - left) along with the morphing wing actuator rotation (second row - right). Figure 11 (in Appendix) shows the generator power response (third row - left) and the rotor speed response (third row - right); power and speed are relatively unaffected while using the morphing wing trailing edge.

Figure 11 (in Appendix) shows the tower base side-to-side moment response (fourth row - left) and the tower base fore-aft moment response (fourth row - right). Both with and without the morphing wing device the responses are along the same order of magnitude. In addition, the LSS torque (see Fig. 11 last row - left, in Appendix) and tower top/yaw bearing yaw moment (last row - right) responses are maintaining level loading while activating the AALC devices.

Tip deflection rate feedback: The same series of runs were also conducted using the rate feedack control system. The numerical results compiled from the FAST runs are shown in Fig. 12 (in Appendix). Similar conclusions can be stated as stated in the previous set of results. The peak moments associated with flap moment response (see Fig. 12 in first row - left, in Appendix) gave a reduction of 25%, see Table 2 for overall comparisons.

Further data reduction for this turbine shown in Figure 8 for the composite rainflow cycle counting results for data gathered at 7, 9, 11, 18 and 24 m/s average windspeeds (six seeds at each windspeed) demonstrates actual reduction in fatigue damage. The windspeed data were combined using a Rayleigh wind speed distribution with average of 5.5 m/s. The composite data show that the numbers of cycles accumulated above 2000 kN-m were eliminated with the use of AALC and the numbers of cycles at lower moments were reduced from the baseline case at all cycle amplitudes.

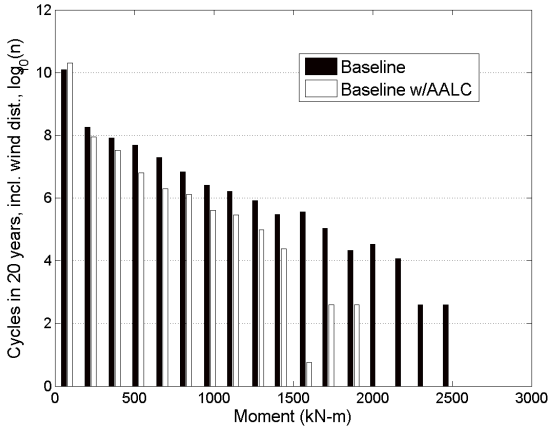

Figure 8. Blade root flap moment rainflow cycle counting results for baseline and active aerodynamic load control (AALC) configurations. 20% chord length flap, $\pm 10^{\circ}$ max. actuation, PD blade tip displacement control.

5.3 5 MW offshore wind turbine [12]

The numerical simulation results from the FAST runs are reported for both conventional *Flaps* (shown in blue) and *No Flaps*

(shown in red) cases. The numerical results compiled from the FAST runs are shown in Fig. 13 (in Appendix). Similar conclusions can be stated as stated in all the previous sets of results. The peak moments associated with the root flap moment response (see Fig. 13 in first row - left, in Appendix) gave a reduction of 20%, see Table 2 for overall comparisons.

Table 2. Root Bending Moment Tabulated Results

WT (MW) (size)	Mean (kNm)	STD (kNM) (no flaps / flaps)	% Red. STD
0.6	206	53.32 / 42.25	21
1.5	603	294 / 199.5	32
1.5 RC	603	294 / 219	25
5.0	4714	2350 / 1880	20

STD is standard deviation about the mean, RC is rate control.

5.4 Increase in Energy Capture by Grow-The-Rotor

By growing the rotor up to where the blade root flap bending moment experiences the same fatigue loads as the baseline, additional energy capture will result. For example, the 1.5 MW WindPACT blades were grown by 10% and the additional energy capture was approximated at 10% (see reference [1]). The corresponding power calculations, as compared to the base without AALC, are shown in Fig. 9, for wind conditions 10 m/s and 11 m/s. An increase of average power generation was calculated that goes from 11% to 7%, over the period of time shown.

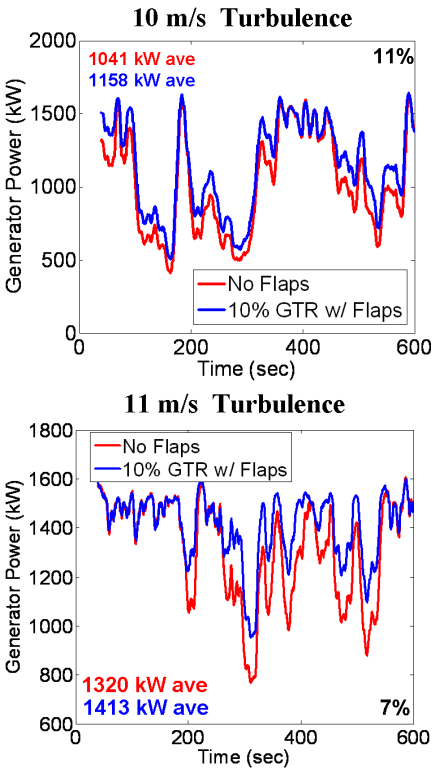

Figure 9. **1.5MW Wind Turbine** power generation numerical simulation results: for baseline and grow-the-rotor, 10 m/s and 11 m/s.

6 Conclusions

This paper has shown the feasibility for employing active aerodynamic devices for load alleviation. Microtabs were simulated with the 600kW NREL CART machine, morphing wing trailing edge devices with 20% chord were simulated with the 1.5 MW WindPACT wind turbine and conventional flaps were simulated with the 5 MW NREL Offshore wind turbine. A PD feedback controller, based on tip deflection, was used for all three wind turbines. In addition, a rate feedback controller, based on tip rate deflection, was used for the 1.5MW WindPACT wind turbine. Both control strategies were shown to be effective for load reduction. The general trend for all turbines showed a decline in root flap bending moments, between 20-32% reduction in the standard deviation oscillations from the mean value. This translates to reduction in the fatigue damage on the wind turbines. It has been demonstrated that active aerodynamic devices may provide substantial benefit for future wind turbine designs by reducing the blade root flap fatigue loads. For example, the designer may elect to: i) increase effective rotor size, ii) extend potential life expectancy and reliability to ultimately reduce the cost-of-energy of future large wind turbine machines. By reducing the blade root flapwise moments with the active aerodynamic devices while keeping drivetrain and tower loads level, the rotor can be grown by increasing the blades until the original fatigue load levels are reached. A methodology for reducing loads and fatigue such that the designer can then *grow the rotor*, by increasing the blade lengths on the turbine, as a way to increase energy capture, is further developed in [1].

ACKNOWLEDGMENT

Sandia National Laboratories is a multiprogram laboratory operated by Sandia Corporation, a Lockheed Martin Company, for the U.S. Department of Energy's National Nuclear Security Administration under contract DE-AC04-94AL85000.

REFERENCES

[1] Berg, D.E., Wilson, D.G., Berg, J.C., Resor, B.R., Barone, M.F., Zayas, J.R., Kota, S., Ervin, G., and Maric, D., *The Impact of Active Aerodynamic Load Control on Wind Energy Capture at Low Wind Speed Sites*, accepted for publication, European Wind Energy Conference & Exhibition, France, March, 2009.

[2] Kelley, N.D., et. al., *The Impact of Coherent Turbulence on Wind Turbine Aeroelastic Response and Its Simulation*, WindPower 2005 Conference, NREL/CP-500-38074, August 2005

[3] Jonkman, J. and Cotrell, J., *Demonstration of the Ability of RCAS to Model Wind Turbines*, National Renewable Energy Laboratory, Golden, CO., NREL/TP-500-34632, 2003.

[4] McCoy, T.J. and Griffin, D.A., *Active Control of Rotor Geometry and Aerodynamics: Retractable Blades and Advanced Devices*, AWEA WINDPOWER 2007 Conference, Los Angeles, CA., June 4-6, 2007.

[5] Yen, D., van Dam, C.P., Smith, R.L. and Collins, S.D., *Active Load Control for Wind Turbine Blades Using MEM Translational Tabs*, Proceedings of the 2001 ASME Wind Energy Symposium (AIAA 2001-0031), Reno, Nevada, January 2001.

[6] Yen Nakafuji, D.T., van Dam, C.P., Michel, J., Morrison, P. *Load Control for Turbine Blades: A Non-Traditional Microtab Approach,* Proceedings of the 2002 ASME Wind Energy Symposium (AIAA 2002-0054), Reno, Nevada, January 2002.

[7] van Dam, C.P., et. al., *Computational and Experimental Investigation into the Effectiveness of a Microtab Aerodynamic Load Control System*, unpublished Sandia Report, August, 2004.

[8] Andersen, P.B., et. al., *Integrating Deformable Trailing Edge Geometry in Modern Mega-Watt Wind Turbine Controllers*, EWEA 2008 European Wind energy Conference & Exhibition, Belgium March 31 - April 3, 2008.

[9] Barlas, T.K. and van Kuik, G.A.M., *State of the Art and Prospectives of Smart Rotor Control for Wind Turbines*, The Science of Making Torque from Wind, J. of Physics: Conference Series 75, 2007.

[10] Wright, A.D. and Fingersh, L.J., *Advanced Control Design for Wind Turbines, Part I: Control Design, Implementation, and Initial Tests*, NREL Technical Report, NREL/TP-500-42437, March 2008.

[11] Malcolm, D.J. and Hansen, A.C., *WindPACT Turbine Rotor Design Study*, NREL Technical Report, NREL/SR-500-32495, June 2002.

[12] Jonkman, J. Butterfield, S., Musial, W., and Scott, G., *Definition of a 5-MW Reference Wind Turbine for Offshore System Development*, NREL Technical Report, NREL/TP-500-38060, February 2009.

[13] Pulliam, T. H., *Efficient Solution Methods for the Navier-Stokes Equations*, Lecture Notes for the von Karman Institute for Fluid Dynamics Lecture Series: Numerical Techniques for Viscous Flow Computation in Turbomachinery Bladings, von Karman Institute, Rhode-St-Genese, Belgium., 1986.

[14] Drela, M. and Giles, M.B. *Viscous-Inviscid Analysis of Transonic and Low Reynolds Number Airfoils*, AIAA J, 25(10):1347-1355, 1987.

[15] Yoo, S.Y. *Integrated Method of CFD and Grid Generation for Automatic Generation of Airfoil Performance Tables*, M.S. Thesis, Mechanical and Aeronautical Engineering Department, University of California-Davis, 2008.

[16] NWTC Design Codes (AirfoilPrep by Dr. Craig Hansen). http://wind.nrel.gov/designcodes/preprocessors/airfoilprep/. Last modified 16-January-2007; accessed 16-January-2007.

[17] Liebeck, R.H., *Design of Subsonic Airfoils for High Lift*, J. of Aircraft, Vol. 15, No. 9, September 1978, pp. 547–561.

[18] van Dam, C.P., et. al., *Active Load Control of Wind Turbine Blades Using Small Tabs or Flaps*, AWEA WINDPOWER 2007, Los Angeles, CA., June 4-6, 2007.

[19] Laino, D.J. and Hansen, A.C., *AeroDyn User's Guide*, prepared for NREL, Windward Engineering, 2002.

[20] Jonkman, J.M. and Buhl, Jr., M.L., *FAST User's Guide*, NREL Technical Report, NREL/EL-500-38230, August 2005.

[21] Kota, S., Hetrick, J.A., Osborn, R., Paul, D., Pendleton, E., Flick, P., and Tilmann, C., *Design and Application of Compliant Mechanisms for Morphing Aircraft Structures*, Smart Structures and Materials 2003: Industrial and Commercial Applications of Smart Structures Technologies, Eric H. Anderson, Editor, Proceedings of SPIE Vol. 5054, 2003.

[22] J.A. Hetrick, J.A., Osborn, R.F., Kota,S., Flick, P.M., Paul, D.B., *Flight Testing of Mission Adaptive Compliant Wing*, 48th AIAA/ASME/ASCE/AHS/ASC Structures, Structural, April 2007, Honolulu, Hawaii, AIAA 2007-1709.

[23] Hand, M.M., Johnson, K.E., Fingersh, L.J., and Wright, A.D., *Advanced Control Design and Field Testing for Wind Turbines at NREL*, The World Renewable Energy Congress VIII, Denver, Colorado, Aug.-Sept., 2004.

[24] Wright, A.D., *Modern Control Design for Flexible Wind Turbines*, NREL Technical Report, NREL/TP-500-35816, July 2004.

[25] Basualdo, S., *Load Alleviation on Wind Turbines using Variable Airfoil Geometry (A 2-D Analysis)*, Technical University of Denmark, Fluid Mechanics Section, Feb. 2004.

APPENDIX: Wind Turbine FAST Simulation Results

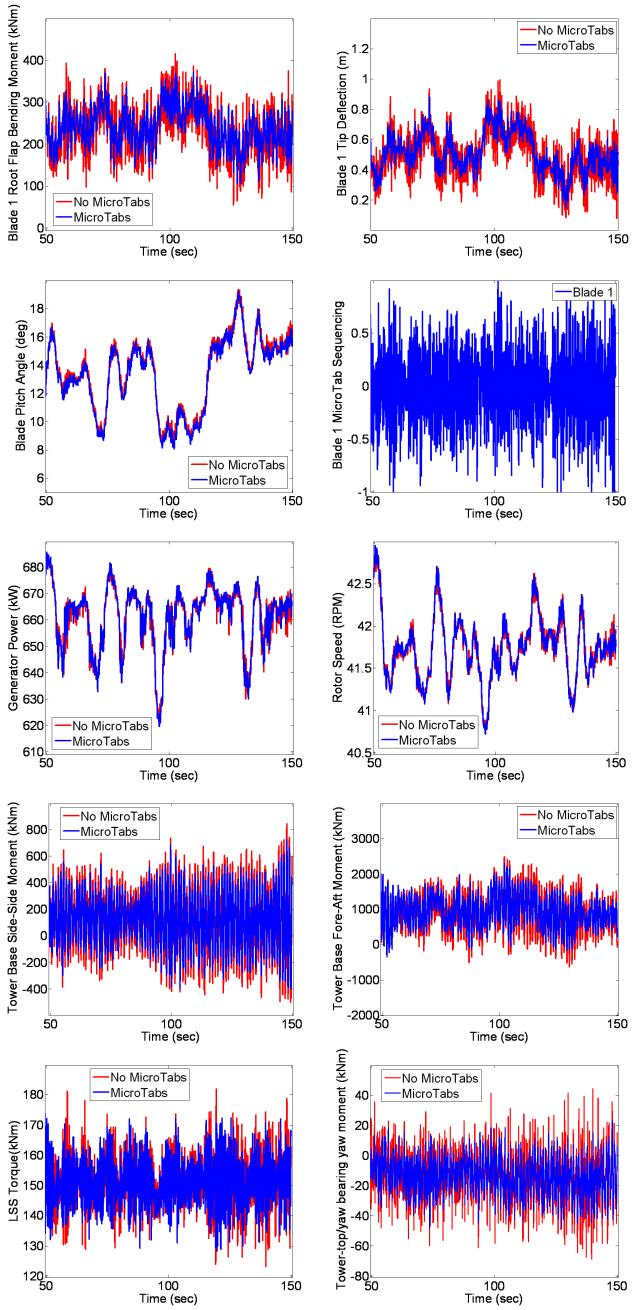

Figure 10. **600kW Wind Turbine** numerical simulation results: first row: blade 1 root flap moment response (left) and blade 1 tip deflection response (right); second row: blade 1 pitch angle response (left) and blade 1 microtab sequencing (right); third row: generator power response (left) and rotor speed response (right); fourth row: tower base side-to-side moment response (left) and tower base fore-aft moment response (right); last row:LSS torque response (left) and tower top/yaw bearing yaw moment response (right)

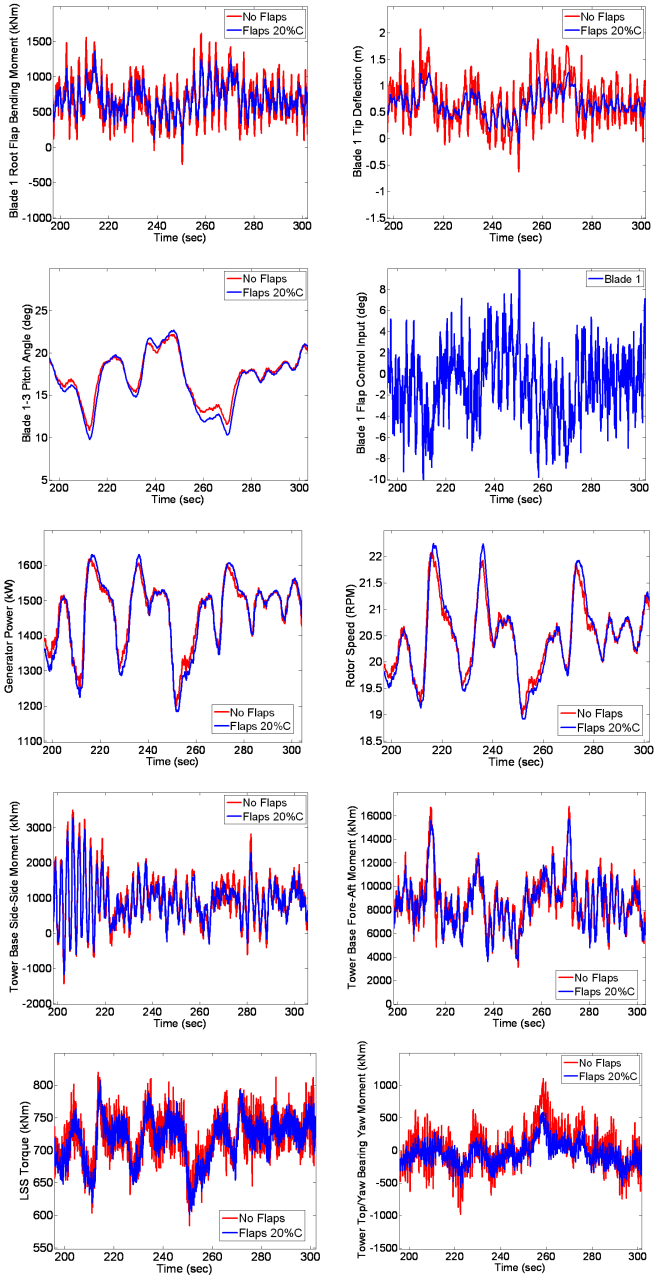

Figure 11. **1.5MW Wind Turbine** numerical simulation results: first row: blade 1 root flap moment response (left) and blade 1 tip deflection response (right); second row: blade 1 pitch angle response (left) and blade 1 microtab sequencing (right); third row: generator power response (left) and rotor speed response (right); fourth row: tower base side-to-side moment response (left) and tower base fore-aft moment response (right); last row:LSS torque response (left) and tower top/yaw bearing yaw moment response (right)

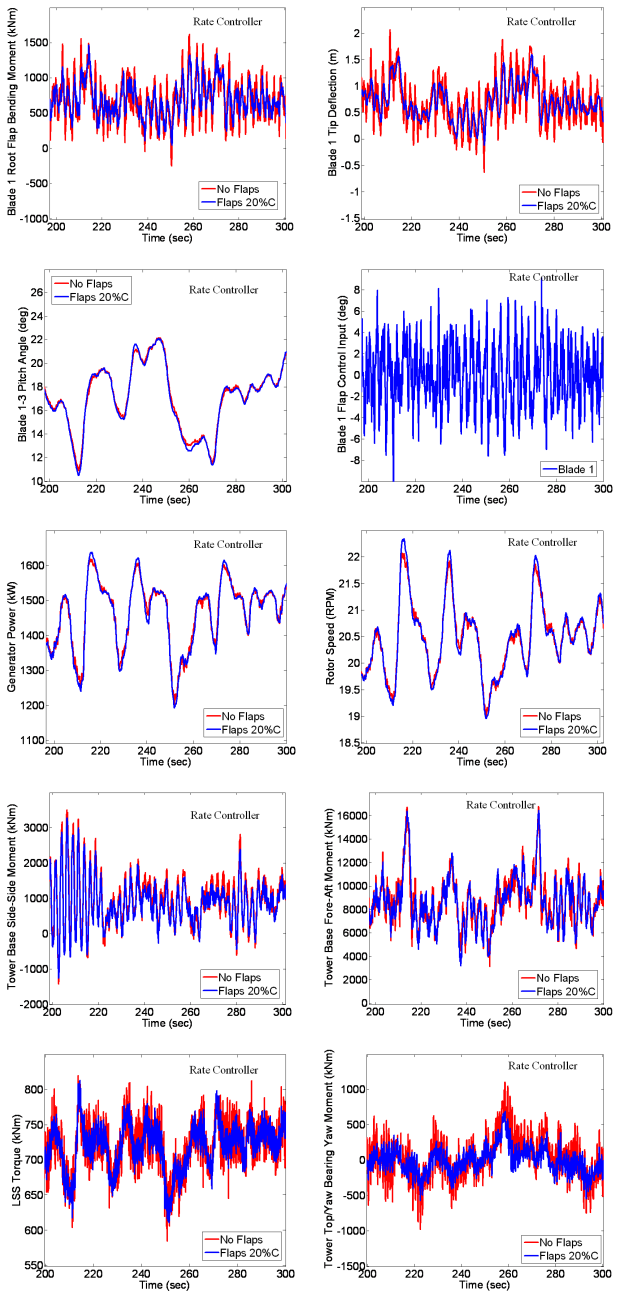

Figure 12. **1.5MW Wind Turbine - Rate Controller** numerical simulation results: first row: blade 1 root flap moment response (left) and blade 1 tip deflection response (right); second row: blade 1 pitch angle response (left) and blade 1 microtab sequencing (right); third row: generator power response (left) and rotor speed response (right); fourth row: tower base side-to-side moment response (left) and tower base fore-aft moment response (right); last row:LSS torque response (left) and tower top/yaw bearing yaw moment response (right)

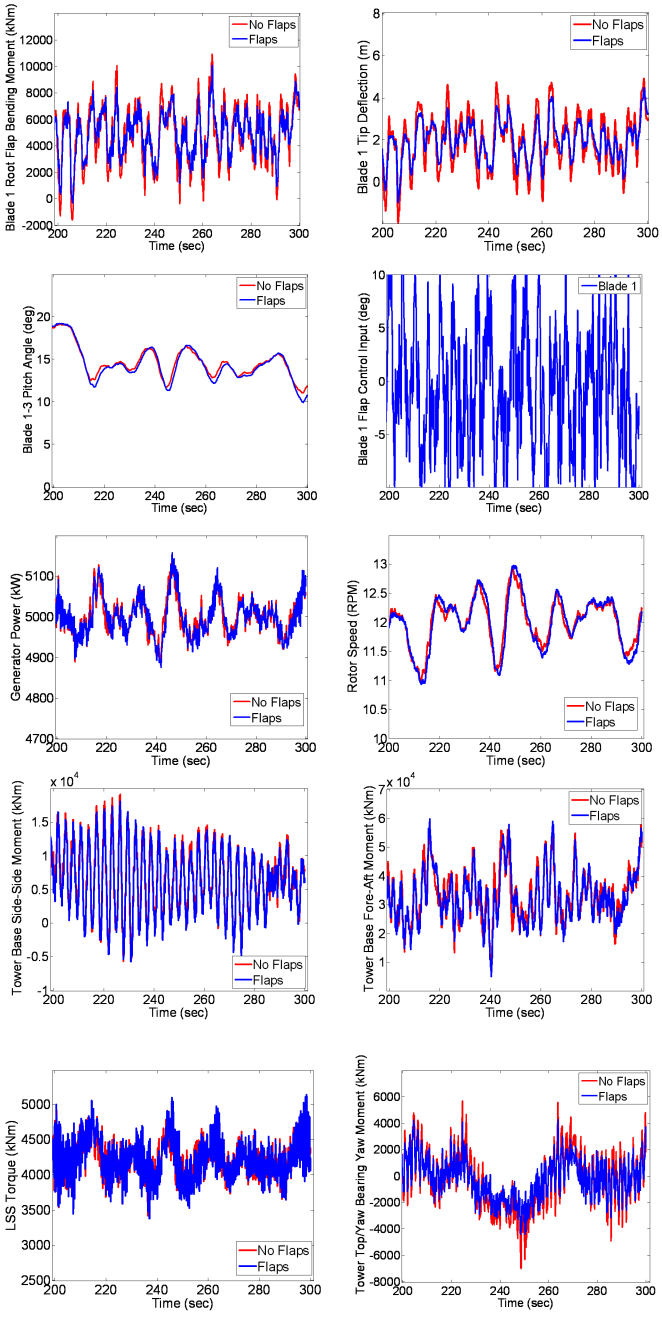

Figure 13. **5 MW Wind Turbine** numerical simulation results: first row: blade 1 root flap moment response (left) and blade 1 tip deflection response (right); second row: blade 1 pitch angle response (left) and blade 1 microtab sequencing (right); third row: generator power response (left) and rotor speed response (right); fourth row: tower base side-to-side moment response (left) and tower base fore-aft moment response (right); last row:LSS torque response (left) and tower top/yaw bearing yaw moment response (right)